Inverse Design of Wind Turbine Blade Sections for Operation under Icing Conditions

Laszlo E. Kollar*
Savaria Institute of Technology
ELTE Eötvös Loránd University, Budapest, Hungary
Károlyi G. tér 4, Szombathely, H-9700, Hungary
e-mail: kl@inf.elte.hu

Rakesh Mishra
School of Computing & Engineering
University of Huddersfield, UK
Queensgate, Huddersfield, HD1 3DH, UK
e-mail: r.mishra@hud.ac.uk

Abstract

A methodology is developed to determine the shape of the two dimensional section of wind turbine blades considering the operation of wind turbine under icing conditions. An inverse design process provides the blade shape from a prescribed pressure or velocity distribution, and then the icing of the blade section obtained is simulated under different ambient conditions. The aerodynamic performances of the bare blade and the iced blade are evaluated and compared, which serves as the basis for involving a correction factor in the inverse design process. This correction factor modifies the prescribed velocity distribution so that the blade shape provided by the inverse design process will be applicable under some icing conditions that are chosen according to the prevailing meteorological conditions of the location where the wind turbine is installed. The procedure presented will contribute towards the design of blade shapes that can enable wind turbines to operate under a wide range of ambient conditions satisfactorily.

Keywords

Aerodynamics; Droplet motion; Icing; Inverse design; Simulation; Wind turbine

1. Introduction

Ice accretion on wind turbine blades in cold climates considerably worsens the aerodynamic performance of the wind turbine. Typically, ice accretion results in reduction of lift generation and increase in drag leading to power loss, which may go up to 50% at sites with particularly high risk of icing [1]. Furthermore, ice accumulation also affects safety and lifetime of the wind turbine systems. Wind speed increases and temperature decreases with altitude in the first several hundred meters above sea level. Moreover, available wind power is higher at lower temperature due to increased air density. Therefore, sites that are optimal for wind farm

* Corresponding author

installation are often exposed to icing events [1]. As protective measures, wind turbines are shut down in case of a threat of heavy ice accretion, or they are equipped with a heating de-icing system that is quite costly [2].

These problems justify the research efforts that had been made to study the effects of icing on wind turbine blades. Both numerical and experimental investigations have been carried out in order to study the ice accretion process on turbine blades and the effects of icing on wind turbine performance. Bose [3] observed ice formation on horizontal axis wind turbine blades, and reported icing profiles that were formed in natural glaze icing events. Fu & Farzaneh [4] modelled the rime-ice accretion process numerically using the commercial CFD code Fluent. They simulated the two-phase flow composed by the cold air and water phases. Then, they estimated the local collision coefficient, and determined the thickness of the accreted ice layer. Turkia *et al*. [5] and Yirtici *et al.* [6] applied numerical approaches to predict power loss due to ice accretion. Kraj & Bibeau [7] simulated icing events experimentally in an icing wind tunnel, and used the data recorded to define the phases of icing on wind turbine blades. Seifert & Richert [8] and Barber *et al*. [9] relied on experimental observations to determine the loss of annual energy production due to ice accretion. Shu et al. [10] studied icing on a small horizontal axis wind turbine numerically and experimentally. They examined the effects of icing on turbine performance, and they also determined the distribution of ice accretion along the blade length. These studies revealed the effects of ice accretion on the aerodynamics of the wind turbine blade, and consequently, on the energy production. Hu et al. [11] investigated how ice mass and ice thickness change along the blade from root to tip, and how they are influenced by the ambient conditions. Ibrahim *et al*. [12] investigated the effects of such blade design parameters as airfoil shape and airfoils thickness on the quantity of ice accumulated on the blade, and they also discussed the effects of ice accretion on the aerodynamic performance of the wind turbine. The present paper will propose a methodology for the design of the blade shape, which takes into account the effects of icing conditions in choosing the blade design parameters.

The aerodynamics of the rotor blades of wind turbines dictates the performance of the wind turbine. The main challenge in the design of rotor blades is to find the relationship between its shape and its aerodynamic properties. In the traditional design process, the designer targets given performance criteria, which is then tested either experimentally or computationally. Then, the geometry is modified based on the results obtained, and the design loop is repeated until an adequate blade design is found. Inverse design methods differ from traditional methods in that geometry is generated automatically for a pre-defined required aerodynamic performance. However, ice accretion on the blade changes the operational geometry, and thereby, it modifies the aerodynamic properties. Careful study of the prevailing icing conditions of the location where the wind farm is installed as well as the effects of icing under those conditions on the aerodynamics of the blade may help improve the process of choosing a blade shape so that the aerodynamic performance degradation due to ice accretion is minimized.

Garabedian & McFadden [13] developed an iterative procedure to design swept wings. This scheme was later modified in [14], which allowed design for a wide range of geometry with prescribed surface pressures. The authors referred to this technique as the modified Garabedian-McFadden (MGM) method. The MGM procedure was incorporated into a multigrid Navier-Stokes airfoil analysis method in [15]. Dulikravich & Baker [16] formulated a Fourier series solution of the MGM equation. The MGM technique was applied in [17] for the inverse design of vertical axis wind turbine blades with constant thickness, which represents a geometry substantially different from those described by airfoils. Kamoun *et al.* [18] presented an inverse design procedure that was adapted to optimise the geometry of the

blade section for a prescribed distribution of bound vortices. Albanesi *et al*. [19] applied the inverse finite element method to design wind turbine blades.

The present paper applies an inverse design methodology for the design of a section of a wind turbine (2D), which is based on the modified Garabedian-McFadden method. Then, the ice accretion on the blade shape obtained is simulated, and the corresponding aerodynamic coefficients are calculated and compared with the coefficients obtained for the bare blade. The results provide information about the extent of increase in drag and reduction in lift due to icing on different blade shapes. It is shown that this aerodynamic performance degradation is related to the difference between velocities near the upper and lower surfaces of the blade. Consequently, a novel correction factor that is a function of this difference between velocities is applied in the inverse design process, which results in a blade shape that undergoes less severe aerodynamic performance degradation due to the ice accumulation. The results obtained provide information for the designer to find the blade shape so that the ice accretion influences aerodynamic performance of the blade minimally, and consequently, the power loss due to icing is reduced.

2. Methodology

The methodology to find a blade shape for a prescribed velocity distribution and to determine the aerodynamic coefficients includes the following steps:

(i) The conventional inverse design process provides the shape of the 2D section of the bare blade for a given velocity distribution.
(ii) The air velocity field is determined in the proximity of the blade obtained.
(iii) The motion of water droplets around the blade is simulated. The local ratio of droplets that hit the blade surface is predicted after considering the collision of droplets to the blade surface. The local ratio of droplets that freeze to the blade surface is calculated from the heat balance, which helps predict the mass and shape of ice accretion at different locations around the blade.
(iv) The air flow around the iced blade is simulated, and the aerodynamic coefficients (i.e. the lift and drag coefficients) are calculated and compared to those obtained for a bare blade.
(v) The ratio of power outputs with and without icing is estimated, and a correction factor is proposed. Consideration of this factor results in a modified velocity distribution, and the application of the inverse design process provides a modified blade shape. This blade shape is expected to provide improved performance under the icing conditions.

The steps (i)-(iii) are implemented in Matlab assuming the potential flow around the blade for bare blade condition. The assumption of potential flow for the flow around the iced blade may induce severe error because of non-uniformity in shape as a consequence of ice accretion hence the ANSYS Fluent computational fluid dynamics software is used in step (iv). After these steps, the ratio of power outputs with and without icing is estimated, and a correction factor is proposed. Consideration of this factor results in a modified velocity distribution, and the application of the inverse design process provides a modified blade shape. The above methodology is repeated assuming different performance criteria (which are satisfied by different blade shapes), as well as different icing conditions.

2.1 Inverse design process

This section describes the modified Garabedian-McFadden technique [14] that is an iterative process to find geometry of the blade according to a required pressure or velocity distribution. An initial blade shape is chosen, and then the positions of blade coordinates are modified so that they approach the positions along the surface that corresponds to the target velocity

distribution. The principle of this technique is that the pressure or velocity distribution near the surface is determined by the surface ordinate y, the slope of the surface dy/dx, and the second derivative of the surface, d^2y/dx^2. The change in the surface ordinate is denoted by Δy. Its positive value means that the profile moves upward on the upper surface and downward on the lower surface. The equation to be solved at each blade position is the following [14]

$$A\Delta y + B\frac{\mathrm{d}(\Delta y)}{\mathrm{d}x} - C\frac{\mathrm{d}^2(\Delta y)}{\mathrm{d}x^2} = V_{tar}^2 - V_{pr}^2 \tag{1}$$

where V_{pr} and V_{tar} are the present and target velocities, respectively, and A, B and C are numerical constants that should be large enough to avoid the airfoil from changing too much in one step. There is no analytical method to choose the constants A, B and C; however, since the change Δy is usually small, its coefficient A should be greater than the other two constants B and C. The effects of the values of these parameters on the number of iterations have been analyzed. The values $A = 1000$; $B = 100$; $C = 400$ were chosen in the present study according to the condition that the number of iterations should be the smallest when the free stream velocity is in the range of interest (i.e. up to 30 m/s, which is the range of velocity prevailing during icing events). When the values were chosen too small (i.e. in the range of 10-100), then the computation did not converge for the higher values of velocities considered. On the other hand, further increase of the values above those listed, did not improve convergence. When the present velocity approaches the target velocity, then the change in the ordinate y reduces, i.e. Δy tends to zero. The upper and lower surfaces of the blade are divided into $n - 1$ subdomains along the chord length during the calculation, then the derivatives in Eq. (1) can be written in discrete form as follows

$$\frac{\mathrm{d}(\Delta y)}{\mathrm{d}x} = \frac{\Delta y_{i+1} - \Delta y_i}{x_{i+1} - x_i}; \qquad \frac{\mathrm{d}^2(\Delta y)}{\mathrm{d}x^2} = \frac{\dfrac{\Delta y_{i+1} - \Delta y_i}{x_{i+1} - x_i} - \dfrac{\Delta y_i - \Delta y_{i-1}}{x_i - x_{i-1}}}{\dfrac{x_{i+1} - x_{i-1}}{2}}; \qquad i = 2,\ldots,n-1 \tag{2}$$

with n denoting the number of points along the upper and lower blade surfaces. The $i = 1$ and $i = n$ positions refer to the first and the last points along the blade (i.e. the leading edge and the trailing edge, respectively). These points do not change their position during the iterative procedure; thus, $\Delta y_1 = \Delta y_n = 0$. Substituting Eq. (2) into Eq. (1) leads to

$$\begin{aligned} &A\Delta y_i + \frac{B}{x_{i+1} - x_i}\Delta y_{i+1} - \frac{B}{x_{i+1} - x_i}\Delta y_i - \frac{2C}{(x_{i+1} - x_i)(x_{i+1} - x_{i-1})}\Delta y_{i+1} \\ &+\left(\frac{2C}{(x_{i+1} - x_i)(x_{i+1} - x_{i-1})} + \frac{2C}{(x_i - x_{i-1})(x_{i+1} - x_{i-1})}\right)\Delta y_i \\ &-\frac{2C}{(x_i - x_{i-1})(x_{i+1} - x_{i-1})}\Delta y_{i-1} = V_{tar}^2 - V_{pr}^2; \qquad i = 2,\ldots,n-1 \end{aligned} \tag{3}$$

If constant step size $\Delta x = x_{i+1} - x_i$ (for each $i = 2, \ldots, n - 1$) is applied, then Eq. (3) becomes

$$k_1\Delta y_{i-1} + k_2\Delta y_i + k_3\Delta y_{i+1} = V_{tar}^2 - V_{pr}^2; \qquad i = 2,\ldots,n-1 \tag{4}$$

where

$$k_1 = -\frac{2C}{(x_i - x_{i-1})(x_{i+1} - x_{i-1})} = -\frac{C}{\Delta x^2}$$

168 $$k_2 = A - \frac{B}{x_{i+1} - x_i} + \frac{2C}{(x_{i+1} - x_i)(x_{i+1} - x_{i-1})} + \frac{2C}{(x_i - x_{i-1})(x_{i+1} - x_{i-1})} = A - \frac{B}{\Delta x} + \frac{2C}{\Delta x^2}$$

$$k_3 = \frac{B}{x_{i+1} - x_i} - \frac{2C}{(x_{i+1} - x_i)(x_{i+1} - x_{i-1})} = \frac{B}{\Delta x} - \frac{C}{\Delta x^2}$$

169 Finally, Eq. (4) for each point $i = 2, \ldots, n-1$ can be organized in the following form

170
$$\begin{bmatrix} k_2 & k_3 & & & 0 \\ k_1 & k_2 & k_3 & & \\ & k_1 & k_2 & \ddots & \\ & & \ddots & \ddots & k_3 \\ 0 & & & k_1 & k_2 \end{bmatrix} \begin{bmatrix} \Delta y_2 \\ \Delta y_3 \\ \Delta y_4 \\ \vdots \\ \Delta y_{n-1} \end{bmatrix} = \begin{bmatrix} V_{tar,2}^2 - V_{pr,2}^2 \\ V_{tar,3}^2 - V_{pr,3}^2 \\ V_{tar,4}^2 - V_{pr,4}^2 \\ \vdots \\ V_{tar,n-1}^2 - V_{pr,n-1}^2 \end{bmatrix} \quad (5)$$

171 The size of matrix in Eq. (5) is $(n-2)$ x $(n-2)$ since the change of position at the leading
172 edge Δy_1 and at the trailing edge Δy_n is zero. It is a tridiagonal matrix; thus, Eq. (5) can be
173 solved by the tridiagonal matrix algorithm or Thomas algorithm [20]. The upper and lower
174 surfaces of the blade are modified according to the solution of Eq. (5). The velocity
175 distribution around this blade is determined, and these velocities are taken into account as
176 present velocities in the next step of iteration. The procedure is repeated until a termination
177 condition is satisfied, i.e. when the average of changes in the position of each point in one
178 side of the blade, related to the blade thickness, became less than a prescribed limit. This
179 average was calculated by summing the changes Δy_i, $i = 2, \ldots, n-1$, then dividing it by the
180 number of points and by the thickness of the initial profile. The limit for the maximum
181 accepted average of changes related to the blade thickness was set at 10^{-4} in the present
182 computation. The flowchart of the computation is shown in Fig. 1, and it includes the
183 following steps:
184 (i) Choose initial blade shape and define flow parameters according to ambient conditions
185 where the wind turbine will be used.
186 (ii) Determine velocity distribution near the blade surface chosen / obtained.
187 (iii) Consider the target velocity distribution and calculate the changes of position $\Delta y_2, \ldots,$
188 Δy_{n-1} as the solution to Eq. (5).
189 (iv) Verify termination condition as described in previous paragraph. If it is not satisfied, then
190 repeat steps (ii)-(iv).
191 (v) If termination condition is satisfied, then blade surface has been found.

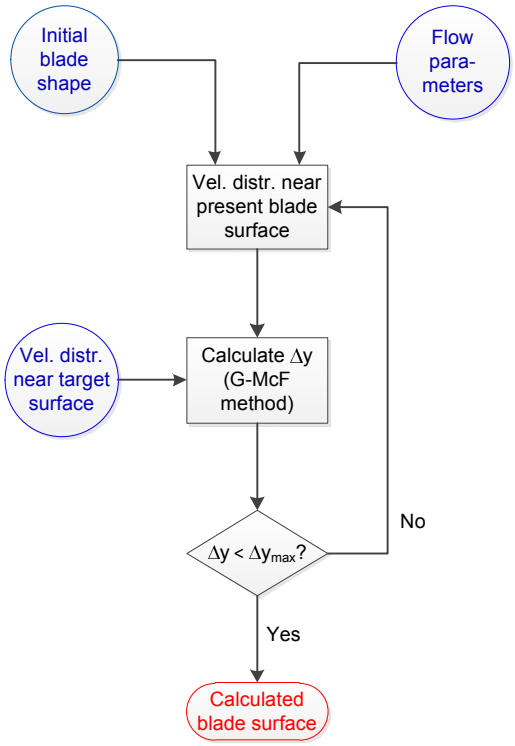

Fig. 1: Flowchart of the computation in the inverse design process

2.2 Air flow around bare blade

The air velocity field in the computational domain around the turbine blade is determined using a panel method [21]. Panel methods solve potential flow over different geometries; thus, it is not applicable to calculate velocities in the boundary layer. However, if the boundary layer is thin, as is the case around airfoils with small angle of attack, then panel methods provide an acceptable approximation of the velocity field. The governing equation is the Laplace's equation for the velocity potential or for the stream function.

The procedure developed in this research applies the panel method that is applicable for 2D, incompressible flow around single-element airfoils where the Laplace's equation is solved for the stream function. The Laplace's equation for the stream function ψ is the consequence of irrotationality, and it is written in the form:

$$\frac{\partial^2 \psi}{\partial x^2} + \frac{\partial^2 \psi}{\partial y^2} = 0 \tag{6}$$

where x and y are coordinates, respectively, parallel with and perpendicular to the blade axis. Eq. (6) is solved by a superposition of elementary solutions. Lifting airfoils can be modelled by vortices, since the circulation around them is non-zero. However, the velocity is singular at the center of vortices; therefore, the vortices should be made as weak as possible in order to produce a smooth flow field. Consequently, vortices of infinitesimal strength $\gamma_0 \mathrm{d}s_0$ are applied in this panel method, where γ_0 is vortex strength per unit length, and $\mathrm{d}s_0$ is length of a small segment of the airfoil. The Laplace's equation is recast into an integral equation. In order to solve the integral equation, the surface is divided into panels, and a control point is chosen at the centre of each panel. It is assumed that the vortex strength γ_0 is piecewise constant on the panels, and then the integral equations are written for the control points. These equations together with the Kutta condition form a system of algebraic equations. The vortices γ_0 on each panel are obtained by solving these equations, and then the velocities are calculated at

any position (x;y) outside the airfoil. Further details of the calculation can be found in textbooks (e.g. [21]). The flowchart of this computation is presented in Fig. 2, and it includes the following steps:

(i) Consider the blade shape obtained in the inverse design process and define flow parameters according to ambient conditions.
(ii) Calculate vortices along the blade and the stream function on the blade surface using the panel method.
(iii) The velocity is zero in the positions (x;y) inside the blade surface.
(iv) Determine the horizontal and vertical components, u and v, of velocity in the positions (x;y) outside the blade surface in the computational domain.

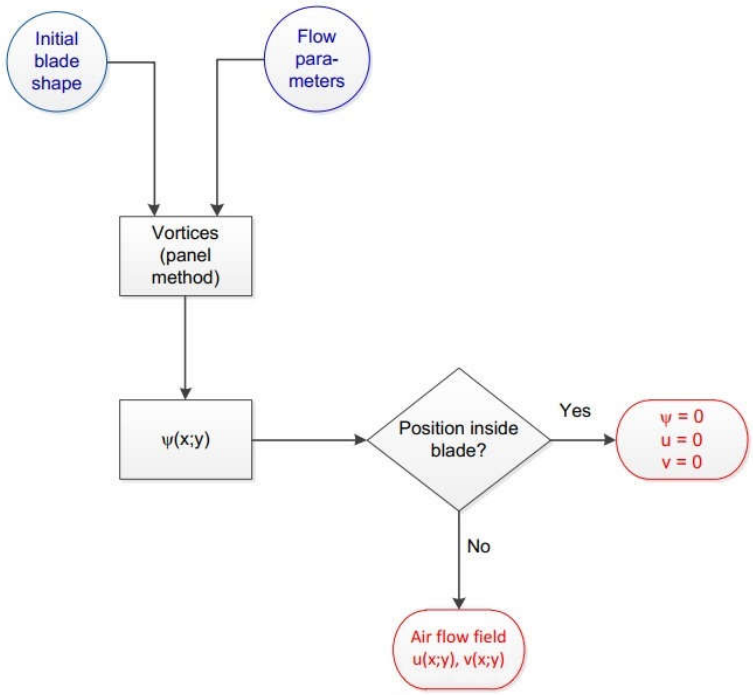

Fig. 2: Flowchart of the computation to determine air flow field around the bare blade

2.3 Mass and shape of ice accretion

Ice accretion is caused by supercooled water droplets that impinge on and freeze at the blade surface. In order to simulate this process, first the droplet trajectories are determined, and local collision efficiencies are calculated along the blade surface. However, not all of the collided droplets freeze to the surface and contribute to the ice accretion. Therefore, the heat balance is applied on the blade surface, which provides the local accretion efficiency along the entire surface. The blade surface was divided into subdomains during the calculation in the inverse design process (see Section 2.1). The total mass of droplets in each subdomain on the surface is multiplied by the local accretion efficiency so that the relative mass and then the relative thickness of ice can be determined locally.

2.3.1 Rate of icing

The maximum flux density of water droplets that may contribute to the ice growth on a unit projection area F is the product of mass concentration w and the velocity v of particles relative to the icing object. The rate of icing, i.e. the accreted ice mass M in unit time t, is expressed in the form [22]

$$\frac{\mathrm{d}M}{\mathrm{d}t} = \alpha_1 \alpha_2 \alpha_3 w v F \tag{7}$$

The maximum flux density is reduced by three correction factors that should be determined in order to obtain the rate of icing. These are (i) the collision efficiency α_1, i.e. the ratio of the flux density of the particles that hit the icing object to the maximum flux density; (ii) the sticking efficiency α_2, i.e. the ratio of the flux density of the particles that stick to the object to the flux density of the particles that hit the object; and (iii) the accretion efficiency α_3, i.e. the ratio of the rate of icing to the flux density of the particles that stick to the object [19]. The simulation of droplet trajectories around the blade provides information about the ratio of the particles that hit the blade surface, from which the collision efficiency is obtained as discussed in Section 2.3.2. If snow accretion is not considered, then the sticking efficiency may be assumed to be 1, because water droplets do not bounce. Finally, the accretion efficiency is obtained from the heat balance of droplets on the blade surface as explained in Section 2.3.3. Since these correction factors are calculated locally along the blade surface, the rates of icing at different positions along the turbine blade and the relative local ice thickness on the blade surface can be determined.

2.3.2 Droplet trajectories and collision efficiency

The motion of water droplets in the cold air is simulated by the Eulerian-Lagrangian approach for two-phase flows. The carrying gas phase is continuous, whereas the liquid phase is considered by dispersed water droplets. Droplet trajectories are obtained from the droplet equation by the calculation detailed in [23] and [24]. Numerical integrations of this equation provide droplet velocity and droplet position in each time step of the calculation. The calculation of a trajectory is terminated if the droplet hits the blade surface, or the droplet reaches the end of the computational domain without hitting the blade.

The local collision efficiency at the point of impact is determined from the ratio of the initial perpendicular separation of trajectories of two nearby droplets to the final separation of their respective impact points on the blade surface [25]. Assume that two droplets leaving from neighbouring initial positions $(x_0;y_{0,j})$ and $(x_0;y_{0,j+1})$ hit the blade surface at positions (x_j,y_j) and (x_{j+1},y_{j+1}), then the local collision efficiency in the interval limited by the latter points is calculated as follows

$$\alpha_1 = \frac{\left| y_{0,j+1} - y_{0,j} \right|}{\sqrt{\left(x_{j+1} - x_j\right)^2 + \left(y_{j+1} - y_j\right)^2}} \tag{8}$$

The local collision efficiency depends on droplet size. The droplet size distribution (DSD) is discretized by dividing the droplet size spectrum into N bins and approximating the diameter of droplets in each bin by the average value of that particular bin. Local collision efficiencies are first calculated for droplets of each size in the DSD considered, i.e. for each bin. Then, the local collision efficiencies have to be calculated in the subdomains that are used in the accretion model. Finally, a local collision efficiency is determined for each subdomain using all the local collision efficiencies $\alpha_{1,i}$ ($i = 1, \ldots, N$) obtained for different droplet sizes in that subdomain. The local collision efficiency for each droplet size is multiplied by the mass-based relative frequency of that droplet size in the DSD $f_{m,i}$ (so that $\sum_{i=1}^{N} f_{m,i} = 1$), and the sum of these products provides the local collision efficiency in subdomain j ($j = 1, \ldots, n$), where n is the number of subdomains:

$$\alpha_{1j} = \sum_{i=1}^{N} \alpha_{1j,i} f_{m,i} \qquad j = 1, ..., n \tag{9}$$

2.3.3 Accretion efficiency

The local accretion efficiency α_3 is determined from the heat balance [22, 25]

$$Q_f + Q_v + Q_a = Q_c + Q_e + Q_l + Q_s \tag{10}$$

where Q_f is the latent heat released during freezing, Q_v is the kinetic heating of air, Q_a is the heat released in cooling the ice from its freezing temperature to the surface temperature, Q_c is the convective heat transfer, Q_e is the evaporative heat transfer, Q_l appears due to the temperature difference between the impinging droplets and the icing surface, and Q_s is heat loss due to long-wave radiation. The latent heat Q_f includes the accretion efficiency; thus, if all the other relevant parameters are substituted into the heat balance then the accretion efficiency can be determined. The flowchart of the computation detailed in Section 2.3 is shown in Fig 3, and it includes the following steps:

(i) Consider the blade shape and the air flow field obtained in the previous phases of calculation, and define wind data and droplet data according to the ambient conditions. Droplets are assumed at the inlet (i.e. the left boundary) of the computational domain.
(ii) Calculate droplet velocity and position after one time step. If the droplet reached neither the blade surface nor the boundary of the computational domain then repeat this step.
(iii) If droplet reached the boundary of the computational domain then save its data. Calculation of trajectory of this droplet finished without hitting the blade surface.
(iv) If droplet reached the blade surface then save its data and collect droplets in different subdomains along the blade surface.
(v) Determine the droplet size distribution, the relative collected mass and thickness in each subdomain, and calculate local collision efficiencies.
(vi) Consider atmospheric conditions and determine accretion efficiency applying the heat balance in each subdomain along the blade surface.
(vii) Determine the relative accumulated mass and thickness in each subdomain, and plot the blade surface with ice accretion.

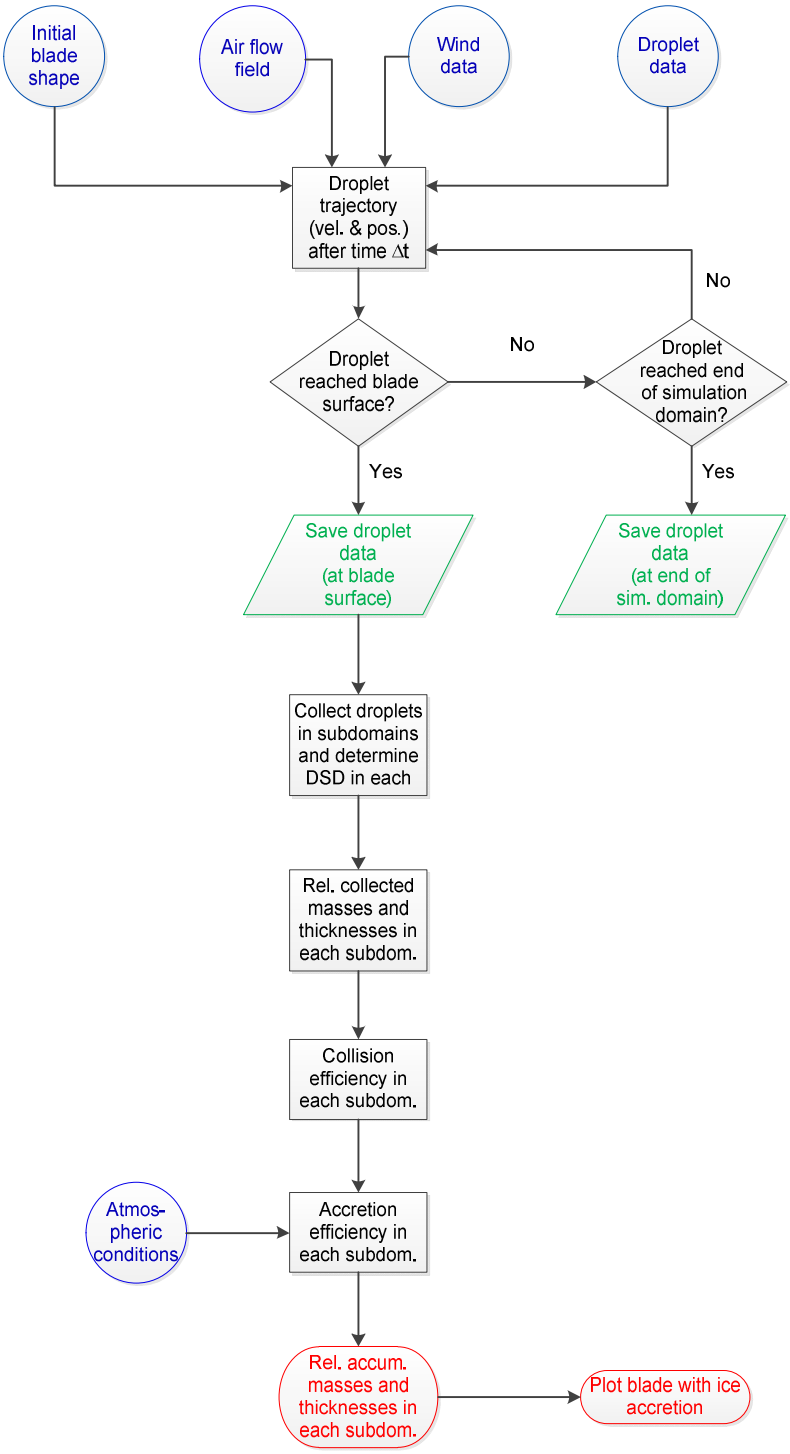

Fig. 3: Flowchart of the computation of icing on the blade surface

The three steps in the procedure as described in Sections 2.1-2.3 are implemented in Matlab, and the flowchart of these computations altogether is shown in the Appendix.

2.4 Air flow around iced blade and aerodynamic coefficients

The shape of iced blade obtained using the computation described in Sections 2.1-2.3 served as input for further computation in order to determine the aerodynamic coefficients. This computation involved the simulation of air flow around the iced blade using ANSYS Fluent computational fluid dynamics software. The computational domain was chosen so that it extended four times the chord length before the leading edge and three times the chord length

after the trailing edge. The height of the computational domain extended twice the chord length above the $y = 0$ position that connects the leading edge and the trailing edge, and twice the chord length below the same position, i.e. 8x4 times the chord length (see Fig. 4). Few simulations were also carried out with a larger and a smaller computational domain. The size of the smaller computational domain was 4x3 times the chord length. In some cases, this smaller domain still provided satisfactory results, but in other cases it affected the accuracy of aerodynamic parameters by more 5%. The size of the larger computational domain was 12x6 times the chord length. Computational cost increased significantly, but the accuracy in the calculation of the aerodynamic parameters was affected by less than 5%. These observations justified the chosen size of the computational domain.

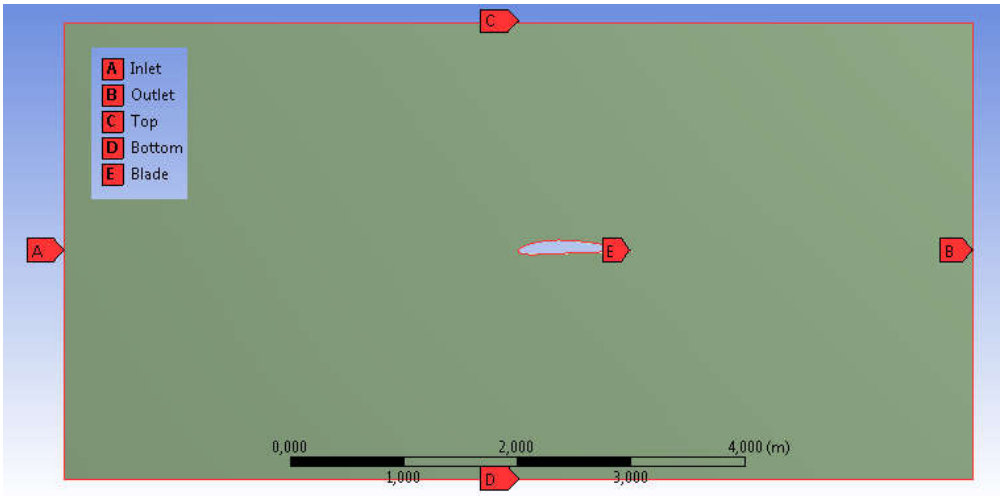

Fig. 4: Computational domain for simulating the flow around the NACA4412 airfoil

Triangular mesh was applied and the minimum and maximum face sizes were chosen as a compromise between accuracy of the aerodynamic coefficients and computational cost. It was also considered that too small elements near the edges of an uneven ice surface as well as too great difference between the minimum and maximum face sizes may lead to loss of convergence. The minimum face size was varied between 0.1% and 0.5% of the chord length, whereas the maximum face size was varied between 1% and 30% of the chord length. The minimum face size was chosen to be 0.1% of the chord length. The maximum face size for the bare blade and for the iced blade was chosen to be 2% and 5%, respectively, of the chord length. Once the maximum face size was fixed, the variation of the minimum face size did not affect the values of aerodynamic coefficients by more than a few %. The mesh in the proximity of the bare NACA4412 airfoil is shown in Fig. 5.

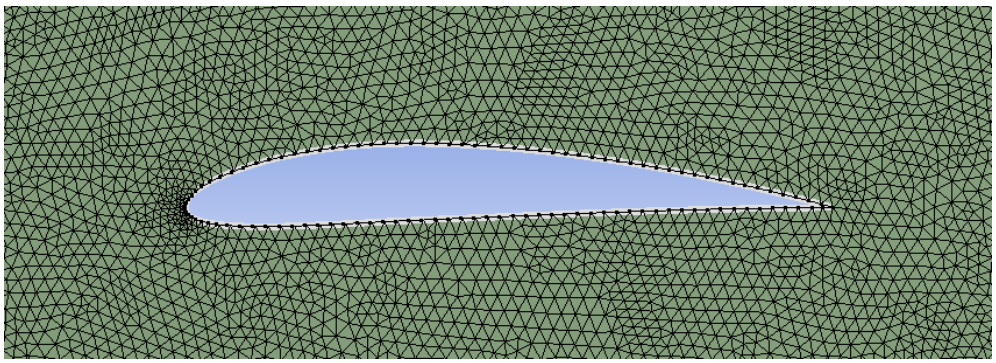

Fig. 5: Mesh around the bare NACA4412 airfoil

The flow was modelled by the k-ε model with standard wall functions. The values of turbulent kinetic energy k and turbulent dissipation ε were determined from the turbulence level and the

characteristic size of turbulent eddy based on the values provided in [24]. The choice of turbulence model was confirmed by [26] where four different turbulence models were applied to simulate the flow around the blades of a horizontal axis wind turbine. They obtained that all of the models considered provided close prediction of the aerodynamic performance for low wind speeds, and that the k-ε model was the most accurate for high wind speeds. Velocity at the inlet of the computational domain was prescribed according to the free stream velocity as boundary condition. Settings of spatial discretization included Green-Gauss node-based gradient evaluation, standard scheme for the pressure equation, and second order upwind scheme for the momentum and energy equations. Solution was initialized from the inlet, and calculation ran for 500 iterations. The simulation results provided the air flow field in the computational domain as well as the drag and lift forces and coefficients.

2.5 Power output and correction factor

The correction factor is determined so that it considers the reduction in energy production due to icing and the frequency of the occurrence of icing events. These issues are taken into account in the calculation of the correction factor by the ratio of power coefficients for the bare and iced blades r_{CP}, as well as the number of icing days per year divided by the number of total days when the wind turbine operates in a year r_{ice}.

The first parameter r_{CP} is determined as follows. The range of wind speeds where operation of wind turbines is considered may be taken from 0 to 25 m/s. When calculating the annual energy production, this range is divided into bins, and the probability of wind speed in each bin is estimated. Typically, the Rayleigh or Weibull distribution may be applied as the probability density function of the wind speed [27]. Then, the power is calculated for each speed v_i as follows

$$P\left(v_i\right)=\frac{1}{2}\rho A v_i^3 C_P \tag{11}$$

Here, ρ is the air density, A is the area swept by the rotor, and C_P is the power coefficient. The energy production is the sum for each wind speed of products of power, the probability of wind speed, and time Δt

$$E=\sum_{i=1}^{N-1} P\left(v_i\right)\cdot f\left(v_i\right)\cdot \Delta t \tag{12}$$

The reduction in energy production due to icing depends on the reduction in the power coefficient C_P. The calculation of this parameter is simplified in the present paper for the maximum power coefficient of a simple lifting translator [28]

$$C_P=\frac{2}{9}C_L\frac{C_L}{C_D}\sqrt{1+\frac{4}{9}\left(\frac{C_L}{C_D}\right)^2} \tag{13}$$

Note that the value obtained by (13) is significantly greater than the power coefficient of a wind turbine, but the correction factor depends on the ratio of power coefficients for the bare and iced cases r_{CP}, and it does not depend on their absolute value.

The second parameter r_{ice} is based on statistics of meteorological data available for the geographical region where the wind turbine is installed. Then, the value of the correction factor r is calculated from the product of the ratio of power coefficients and the frequency of the occurrence of icing events

$$r=1+r_{CP}r_{ice} \tag{14}$$

The application of correction factor changes the blade shape, and consequently, the velocity distribution around the bare blade. The benefit is that the aerodynamic performance degradation of the blade due to ice accretion is reduced significantly; however, the disadvantage is that the aerodynamic performance under no-icing conditions will also be altered due to the modified velocity distribution. Therefore, the correction factor should influence the blade shape only if it is justified by the severity and frequency of icing conditions. If ice does not change the aerodynamics of the blade significantly or icing events are rare, then the parameters r_{CP} or r_{ice} are so small that the correction factor will approximately be one. This means physically that the target velocity distribution, and consequently, the blade shape will not be affected by icing conditions.

3 Validation

3.1 Test of the inverse design process

The inverse design process was applied to obtain blade shapes with substantially different lift coefficients. In this test, the velocity distributions around NACA1412 and NACA8412 airfoils were calculated, and then these velocity distributions were chosen as target velocity distributions for the inverse design process in order to verify if the shapes of the same airfoils will be obtained. The first digit in the code of NACA 4-digit airfoils refers to the maximum distance between the camber line and the horizontal line connecting the leading edge and the trailing edge. Thus, when this number increases, the shapes become more asymmetric, and consequently, the blades cause higher flow turning at the trailing edge, which results in greater lift. The velocity distribution around the symmetric NACA0012 airfoil was chosen as initial velocity distribution. The air velocity was 10 m/s, and the angle of attack was zero degrees. Fig. 6 shows that the inverse design process can provide an excellent fit for the shape that is known in advance in the test (cf. curves “calculated” and “target” in Figs. 6(a) and (b)), and that the process is reliable even if the initial velocity distribution and the corresponding blade shape are substantially different from the target velocity distribution and blade shape (see Fig. 6(b)). The inverse design process found the blade shapes in all the cases quickly, i.e. after 20-70 iterations when both of the top and bottom blade surfaces are divided into 50 subdomains, i.e. both surfaces contained 51 points including the points at the leading edge and at the trailing edge, and the average error in the position of these subdomains is set at 10^{-4} times the thickness of the airfoil. Note that when choosing the number of subdomains, it was considered that the calculation in the inverse design process should converge, but the choice was also based on a compromise in the simulation of icing. Realistic iced shape cannot be obtained if the number of subdomains is too low; and, on the other hand, very few droplets freeze in each subdomain if their size is too small, i.e. their number is too high, which enhances the effects of the calculation error.

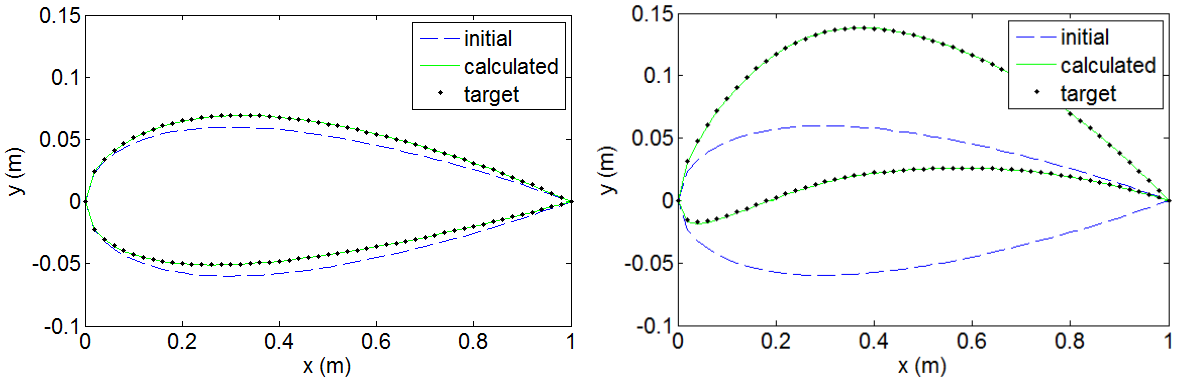

(a) (b)

Fig. 6: Initial, target and calculated blade shapes when the target velocity distribution was defined from that around (a) NACA1412 airfoil; (b) NACA8412 airfoil

3.2 Evaluation of the ice accretion model

The mass and shape of ice accreted on the blade surface is influenced by the ambient conditions. This section discusses the effects of varying the air temperature and the liquid water content (LWC), and compares the tendencies with those obtained in [25] and [29].

The ice shapes on the NACA4412 airfoil are shown in Fig. 7 for different air temperatures between –5 °C and –15, while other thermodynamic parameters are kept constant. It may be observed that the ice accretion is more concentrated in the proximity of the leading edge as the air temperature is lower. Similar tendency can be seen in the relevant figures in [25]. However, exact comparison of the ice shapes is not possible, because the airfoil and further ambient conditions were different in [25].

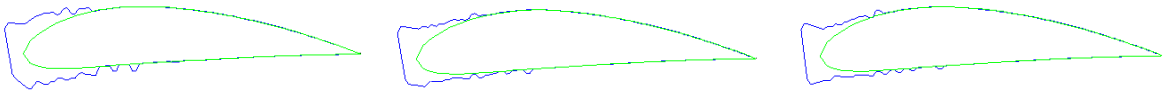

(a) $T_a = -5\,^{\circ}\mathrm{C}$ (b) $T_a = -10\,^{\circ}\mathrm{C}$ (c) $T_a = -15\,^{\circ}\mathrm{C}$

Fig. 7: Effects of air temperature T_a on ice accretion on NACA4412 airfoil, for wind speed of 10 m/s, LWC of 1.5 g/m^3, and median volume diameter of 62 μm

The effects of LWC was also studied on the NACA4412 airfoil shape. Ice accretion is presented in Fig. 8 for different values of LWC, while other thermodynamic parameters are kept constant. Figures clearly show that the quantity of ice increases with LWC. The area on the blade surface with ice accretion increases, but the growth is most apparent in the proximity of the leading edge. This tendency corresponds to the findings of [29]. Again, tendencies only can be compared, because further conditions were different in the literature referred.

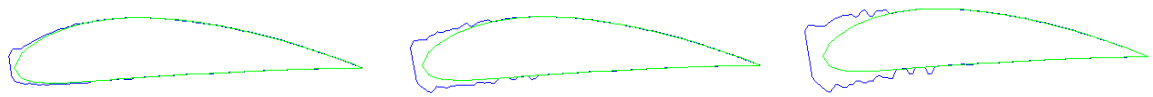

(a) LWC of 0.5 g/m^3 (b) LWC of 1.0 g/m^3 (c) LWC of 1.5 g/m^3

Fig. 8: Effects of LWC on ice accretion on NACA4412 airfoil, for air temperature of –5 °C, wind speed of 10 m/s, and median volume diameter of 62 μm

Lozowski et al. [29] also reported the effects of wind speed. They observed horny shapes for high velocities. However, they investigated aircraft icing; therefore, they considered velocities significantly higher than 30 m/s, which is the highest velocity in the present study. Horny shapes did not occur for this velocity, which is in agreement with the results of the present simulations.

4. Investigation for determination of correction factor

A key point of the methodology proposed is the application of the correction factor. Therefore, its determination requires a comprehensive investigation. One of the most important issue that the correction factor is based on is the reduction in energy production due to icing. Consequently, the following relationships will be studied in this section: (i) relationship between the blade shape and the velocity distributions around the blade surface; as well as (ii) relationship between the blade shape and the aerodynamic performance degradation due to icing. This investigation will provide more knowledge on how the velocity distribution, i.e. the performance criteria that the turbine designer specifies and the correction factor influences as well, affects the reduction in power output or in energy production due to icing.

4.1 Velocity distributions around blade surface

Performance criteria are defined by the velocity distribution around the blade surface. Target velocity distributions are chosen in this section so that they can be produced around blades with significantly different shapes, and the lift coefficients of these blades also differ from each other. The inverse design process was applied for eight velocity distributions. The resulting blade shapes are among the NACA 4-digit airfoils, which were also used in the test in Section 3 and which are listed in Table 1 together with the lift and drag coefficients obtained for angle of attack of zero degrees. Drag coefficient cannot be calculated when the air flow is determined using the panel method; therefore, the air flow around the bare blade was also simulated using the ANSYS Fluent computational fluid dynamics software in order to determine lift and drag coefficients. Three of the velocity distributions are drawn in Figs. 9-11, together with the airflow field around the resulting airfoils for free stream velocity of 10 m/s. These cases were chosen so that they include the two extreme cases, i.e. the shape with the smallest and greatest lift, and one case in between. According to the velocity distributions in Figs. 9-11, the difference between velocities near the upper and lower surfaces at a given position along the chord length increases as the shape becomes more asymmetric. In reality, velocity near the surface means velocity at the limit of the boundary layer, which is small near such a streamlined body as the bare blade. The velocity difference will be described by the following parameter

$$\tilde{v} = \max \frac{v_{up} - v_{ave}}{v_{ave}} \tag{15}$$

Here, v_{up} and v_{ave} denote the velocity at the upper surface and the average of the velocities at the upper and lower surfaces, respectively. The maximum refers to the position along the chord length, where this parameter is maximum, or in other words, where the difference between the velocities near the upper and lower surfaces is maximum. E.g. in Figs. 9-11, the position of the maximum is $x = 0.34$ m, and the value of the parameter $\tilde{v}$ takes 0.038, 0.150 and 0.293, respectively.

Table 1: Blade shapes obtained for different velocity distributions and corresponding aerodynamic coefficients (free stream velocity: 10 m/s; angle of attack: 0 deg)

velocity distribution	blade shape (airfoil)	lift coefficient C_L	drag coefficient C_D	lift-to-drag ratio C_L/C_D
1	NACA1412	0.108	0.0167	6.49
2	NACA2412	0.215	0.0171	12.55
3	NACA3412	0.329	0.0179	18.36
4	NACA4412	0.434	0.0191	22.74
5	NACA5412	0.533	0.0213	25.01
6	NACA6412	0.648	0.0221	29.32
7	NACA7412	0.760	0.0251	30.28
8	NACA8412	0.835	0.0286	29.20

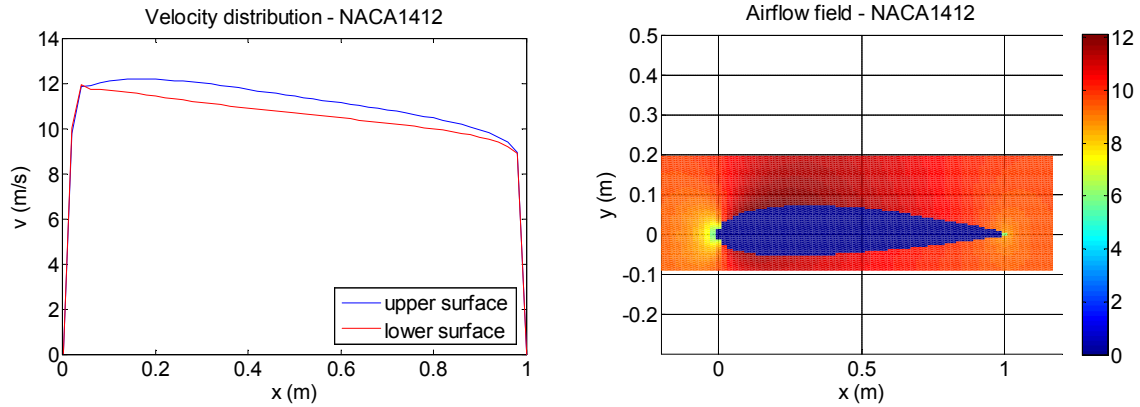

Fig. 9: Velocity distributions near upper and lower blade surfaces and airflow field around NACA1412 airfoil; x, y are coordinates parallel with and perpendicular to chord length, v is velocity, colour bar shows velocity in m/s

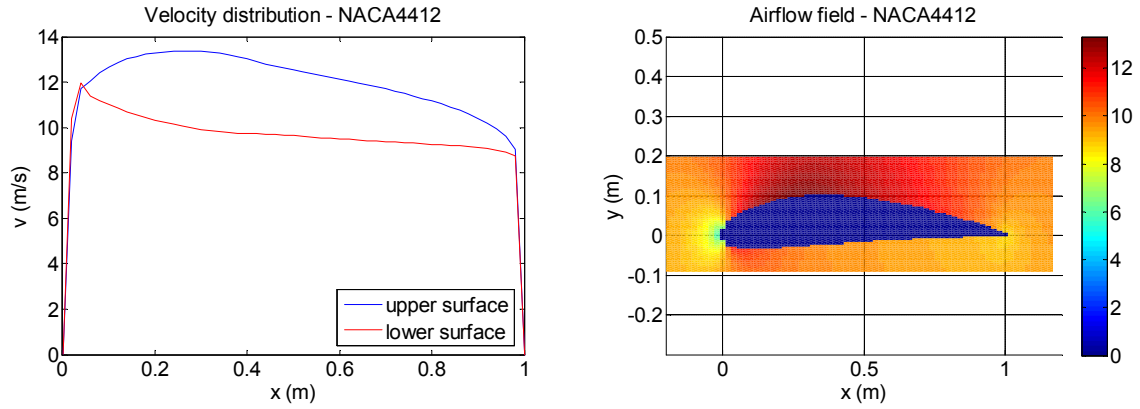

Fig. 10: Velocity distributions near upper and lower blade surfaces and airflow field around NACA4412 airfoil; x, y are coordinates parallel with and perpendicular to chord length, v is velocity, colour bar shows velocity in m/s

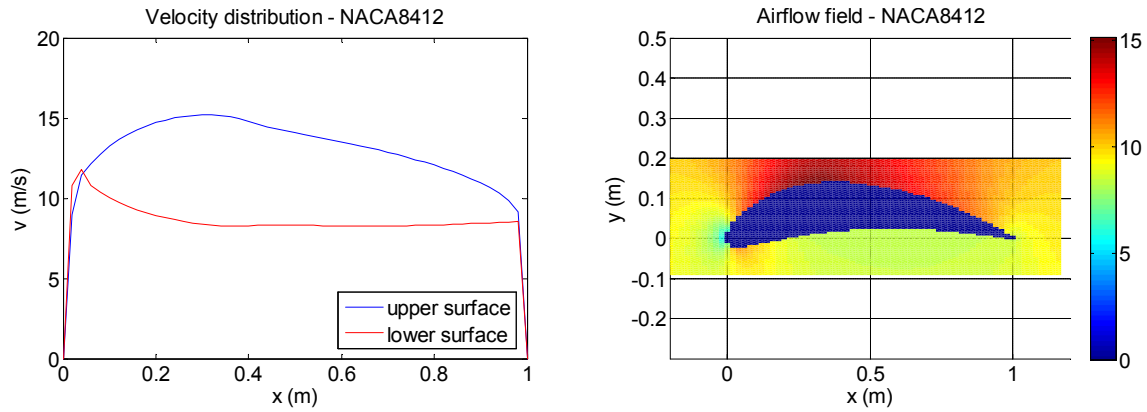

Fig. 11: Velocity distributions near upper and lower blade surfaces and airflow field around NACA8412 airfoil; x, y are coordinates parallel with and perpendicular to chord length, v is velocity, colour bar shows velocity in m/s

4.2 Effects of icing on aerodynamic coefficients

The effects of ice accretion on the aerodynamics of the wind turbine blade are evaluated by comparing the lift and drag coefficients of the bare and iced blades. Ice on the blade decreases the lift coefficient and increases the drag coefficient; however, the extent of modification in these aerodynamic parameters depends on the icing conditions and the blade shape that is determined by the performance criteria. The altered values of the aerodynamic coefficients results in reduced power output and energy production.

Although meteorological conditions vary to some extent everywhere, typical icing conditions may be observed in the geographical location where the wind turbine under examination is situated. If the prevailing icing conditions of the geographical location are considered in the process to determine blade shape, then the rate of reduction in lift and the rate of increase in drag can be reduced. If the prevailing icing conditions occur frequently in the location of the wind turbine, it may be favourable to modify the velocity distribution so that icing on the resulting blade shape leads to less severe aerodynamic performance degradation. In this case, however, the performance of the bare blade under no-icing conditions may not be optimal; thus, the turbine designer must assess to what extent it may be worth altering the target velocity distribution.

The type, mass and shape of ice accreted on the blade depends on the ambient conditions. The ambient conditions chosen in this study correspond to two substantially different icing events: in-cloud icing and freezing drizzle. Typical values of the thermodynamic parameters describing these conditions are listed in Table 2. The wind speed, air temperature and LWC were entered as input variables in the procedure, together with the droplet size distribution in typical clouds under these conditions. The droplet size distribution was measured in a former study [24], and its median volume diameter is presented in Table 2.

Table 2: Thermodynamic parameters describing the icing conditions simulated

Icing condition	Wind speed	Air temperature	Liquid water content	Median volume diameter
	(m/s)	(°C)	(g/m^3)	(μm)
In-cloud icing	20	–10	0.3	27
Freezing drizzle	10	–5	1.5	62

The shape of ice accretion on the blade vary essentially with the blade shape and with icing conditions. The effects of thermodynamic parameters describing the meteorological conditions on the mass and shape of ice accretion have been studied extensively, see e.g. [29]. This section presents the ice shapes obtained on the blades defined by the NACA airfoils listed in Section 4.1 under the two icing conditions defined in Table 2. Then, the aerodynamic performance degradation, i.e. reduction of lift coefficient and increase of drag coefficient, due to ice accretion is discussed.

The ice accretions on the three blade shapes that are also presented in Figs. 9-11 are shown in Figs. 12-14 under in-cloud icing and under freezing drizzle conditions. It can be observed in these figures that the blade shape changes more significantly under freezing drizzle conditions than under in-cloud icing conditions. Consequently, the aerodynamic coefficients also change to a greater extent under freezing drizzle conditions. The lift coefficient C_L decreases, whereas the drag coefficient C_D increases. These changes will be evaluated altogether by the variation of one parameter: the ratio of lift and drag coefficients C_L/C_D. Tables 3 and 4 list the values of this parameter for different blade shapes under the conditions of in-cloud icing and freezing drizzle, respectively. The values are slightly different under the two conditions even for the bare blade, because the parameters in the turbulence model are also different under those conditions (see Section 2.4 and [24]). Tables 3 and 4 also reveal in their last columns to what extent the ratio of lift and drag coefficients as well as the power coefficient calculated by Eq. (13) are reduced due to ice accretion. As expected, the reduction is significantly greater under freezing drizzle conditions than under in-cloud icing conditions.

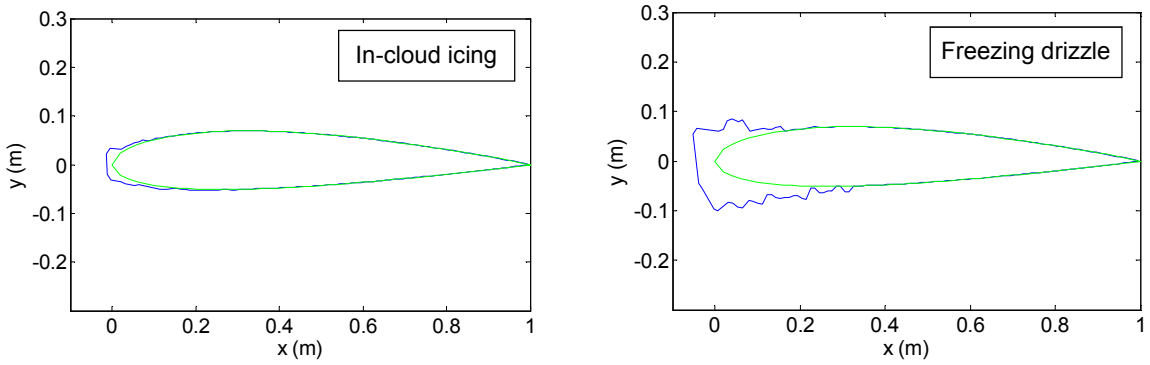

Fig. 12: Iced shapes of NACA1412 under in-cloud icing and freezing drizzle conditions

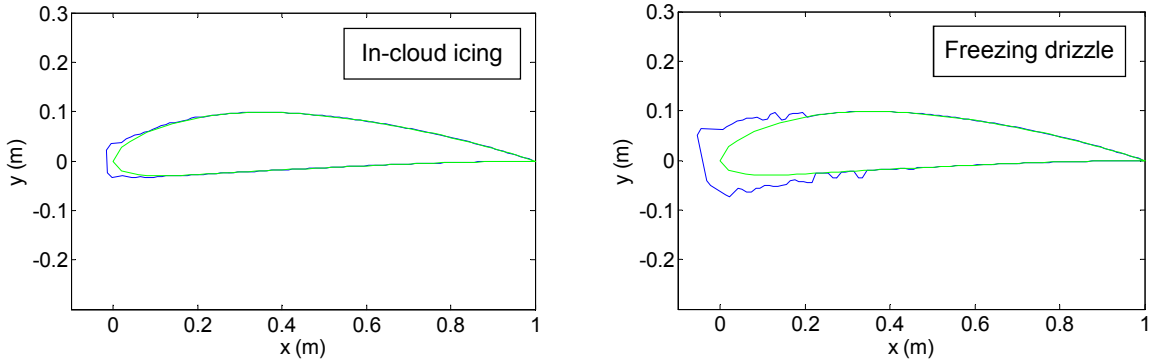

Fig. 13: Iced shapes of NACA4412 under in-cloud icing and freezing drizzle conditions

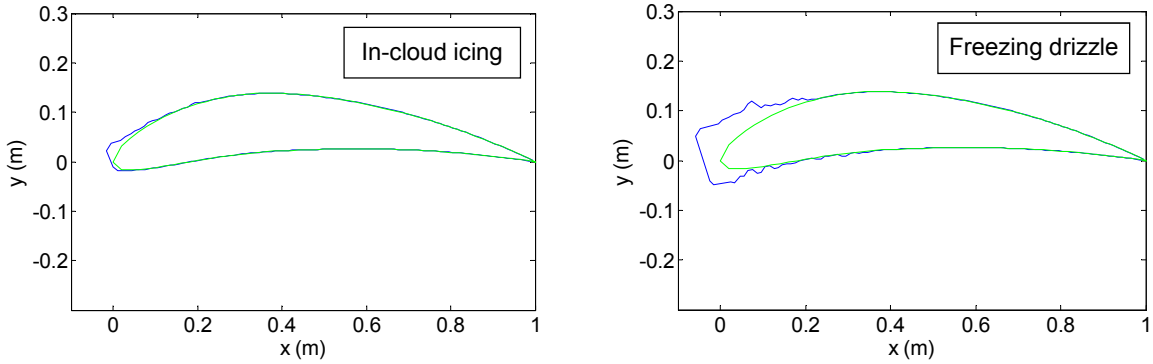

Fig. 14: Iced shapes of NACA8412 under in-cloud icing and freezing drizzle conditions

Table 3: Aerodynamic coefficients under in-cloud icing conditions, C_L: lift coefficient, C_D: drag coefficient, C_P: power coefficient for lifting translator

Aerofoil	$(C_L/C_D)_{\text{bare}}$	$(C_L/C_D)_{\text{iced}}$	$\frac{(C_L/C_D)_{\text{iced}}}{(C_L/C_D)_{\text{bare}}}$	$\frac{C_{P,\text{bare}}}{C_{P,\text{iced}}}$
NACA1412	7.49	3.63	0.484	5.34
NACA2412	14.20	6.90	0.486	4.27
NACA3412	18.63	13.01	0.698	1.98
NACA4412	24.12	16.07	0.666	2.20
NACA5412	27.68	22.01	0.795	1.45
NACA6412	32.39	24.49	0.756	1.68
NACA7412	37.31	27.50	0.737	1.84
NACA8412	34.50	26.47	0.767	1.70

Table 4: Aerodynamic coefficients under freezing drizzle conditions, C_L: lift coefficient, C_D: drag coefficient, C_P: power coefficient for lifting translator

Aerofoil	$(C_L/C_D)_{\text{bare}}$	$(C_L/C_D)_{\text{iced}}$	$\frac{(C_L/C_D)_{\text{iced}}}{(C_L/C_D)_{\text{bare}}}$	$\frac{C_{P,\text{bare}}}{C_{P,\text{iced}}}$
NACA1412	6.49	0.77	0.119	60.3
NACA2412	12.55	1.53	0.122	66.1
NACA3412	18.36	4.25	0.232	21.6
NACA4412	22.74	6.70	0.294	14.1
NACA5412	25.01	8.63	0.345	9.42
NACA6412	29.32	9.11	0.311	12.4
NACA7412	30.28	13.86	0.458	5.00
NACA8412	29.20	13.34	0.457	5.06

It was reported in a former study [30] that the ratio C_L/C_D for the iced blade is reduced to 10-30% of the same ratio for the bare blade under freezing drizzle conditions; whereas it is reduced approximately to 50% under in-cloud icing conditions. In both cases, the reduction was more severe for closely symmetric shapes as well as for greatly asymmetric shapes; and the aerodynamic degradation was less severe for a blade shape in between. Since more shapes have been examined in the present study, this latter observation may be formulated more accurately. When the blade shape is closely symmetric (e.g. NACA1412 airfoil), then ice accretion worsens aerodynamic properties to the greatest extent (reduction of the ratio C_L/C_D under freezing drizzle and in-cloud icing conditions, respectively, to 12% and 48% of the same ratio for bare blade). As

the profile becomes more asymmetric, the extent of reduction in the ratio C_L/C_D will be smaller (or, in other word, the value in Column 4 of Tables 3 and 4 will be greater). However, this behaviour cannot be improved without any limit. Asymmetric profiles are associated with greater values of the ratio C_L/C_D, but this value does not change significantly for the most asymmetric profiles considered, i.e. for NACA5412-NACA8412 airfoils (cf. the values in the bottom half of the last column in Table 1). The reduction in the ratio C_L/C_D due to ice accretion will also remain in approximately the same range for these blades (i.e. to ca. 70% under in-cloud icing and to ca. 40% under freezing drizzle, as shown in Tables 3 and 4, respectively).

4.3 Calculation of correction factor

This section explains the calculation of the correction factor for modifying the target velocity distribution, which is proposed in the inverse design process when icing conditions occur frequently in the location where the wind turbine will operate. The definition of this correction factor is provided by Eq. (14), and its value is based on two observations made in Sections 4.1 and 4.2. First, the difference between velocities near the upper and lower surfaces at a given position along the chord length increases with the first digit in the NACA airfoil, i.e. it is greater for asymmetric shapes providing greater lift (cf. velocity distributions in Figs. 9-11). Second, the reduction in the lift-to-drag ratio and in the power coefficient is less severe for these asymmetric shapes. Thus, if the differences between velocities near the upper and lower surfaces in the target velocity distribution are small (i.e. the value of $\tilde{v}$ defined by Eq. (15) is not greater than 0.1), then a significant reduction can be expected due to ice accretion in the lift-to-drag ratio and in the power coefficient, and it may be advisable to increase the difference between the velocities near the upper and lower surfaces. The extent of this increase depends on several circumstances that the designer should consider, including the target velocity distribution, the prevailing icing conditions in the location of the wind turbine, and the frequency of occurrence of the icing event. The value of correction factor may be greater than or equal to one. If it is equal to one, it means that the target velocity distribution determined for no-icing conditions will not be changed at all in the inverse design process. This decision is justified if the risk of icing is so low that it is not advantageous to take it into account (i.e. $r_{ice} = 0$ in Eq. (14)). If its value is greater than one, then the target velocity distribution is modified as follows. The difference between the velocities near the upper and lower surfaces of the blade (or the parameter $\tilde{v}$) is multiplied by the value of the correction factor. This means that the average of the velocities at the upper and lower surfaces at a given location does not change, but the velocities near the upper and lower surfaces are modified according to the following formulae:

$$v_{up,m} - v_{ave} = r\left(v_{up} - v_{ave}\right) \tag{16a}$$

$$v_{ave} - v_{low,m} = r\left(v_{ave} - v_{low}\right) \tag{16b}$$

where v_{up} and v_{low} are the velocities near the upper and lower surfaces, respectively, before the application of the correction factor, and $v_{up,m}$ and $v_{low,m}$ are the velocities near the upper and lower surfaces, respectively, after the application of the correction factor. Thus, the obtained modified target velocity distribution results in a more asymmetric blade profile that produces greater lift, and in a less severe aerodynamic degradation due to ice accretion. According to the definition (14), the correction factor is determined by two ratios:

- The ratio of power coefficients for the bare and iced cases, r_{CP}, considers the effects of the target velocity distribution and the prevailing icing conditions in the location of the wind turbine.
- The ratio of the number of icing days per year and the number of total days when the wind turbine operates in a year, r_{ice}, considers the effects of the frequency of the occurrence of

icing events. This can be predicted based on statistics of meteorological data and icing maps.

The value of the correction factor cannot be smaller than one, but there is no theoretical limit for its maximum. It may reach ten in extreme cases, e.g. when the ratio of power coefficients exceeds 60 (see Table 4), and the number of icing days a year is great (50-60).

5 Case study for inverse design involving correction factor

As an example, the correction factor is determined for a particular case, and the inverse design is applied involving the correction factor obtained. Assume that the prevailing icing event is freezing drizzle, and the expected number of icing days during the winter season is 15 in the location of the wind turbine. The target velocity distribution is given so that it can be produced by a NACA1412 airfoil (this can be determined by the inverse design process without correction factor). The recommended value of correction factor in this case is determined from Eq. (14) with $r_{CP} = 60.3$ (see Table 4) and $r_{ice} = 15/365 = 0.041$ (assuming that the wind turbine can operate during the whole year):

$$r = 3.5 \tag{17}$$

The target velocity distribution, the blade shape obtained by the inverse design process, and icing on the shape obtained can be compared in Figs. 15 and 16, respectively, with and without the application of the correction factor. The lift-to-drag ratio would reduce from 6.49 for bare blade to 0.77 for iced blade without correction factor (i.e. by a ratio of more than 8), whereas it reduces from 22.19 to 4.69 with the application of the correction factor (i.e. by a ratio of less than 5). The ratio of power coefficients for the bare and iced cases would be 60.3 without correction factor, whereas this ratio changes to 27.7 if the correction factor is involved in the inverse design process. In other words, the power loss during the icing days is still great, but it is significantly smaller than that with the blade shape obtained without application of the correction factor. These results show that the aerodynamic performance degradation due to ice accretion is significantly less severe when the correction factor is involved in the inverse design process.

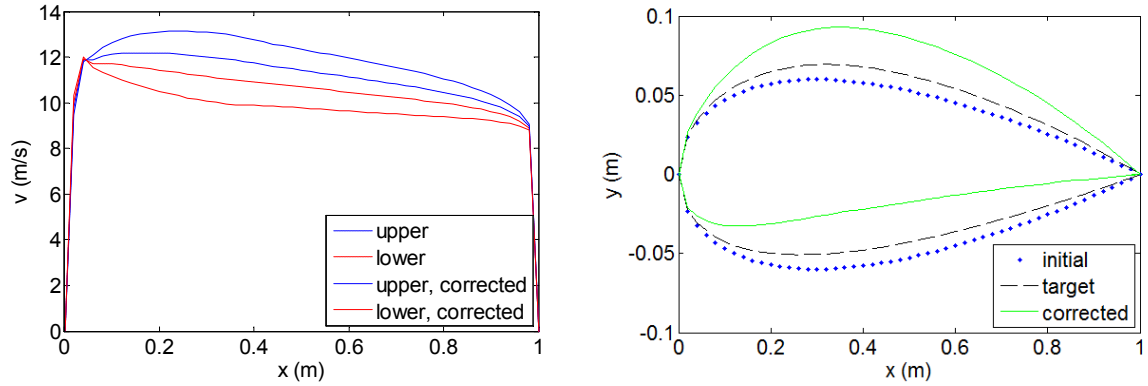

(a) (b)

Fig. 15: (a) Target velocity distributions without (dashed line) and with (solid line) correction factor; (b) blade shapes obtained by the inverse design process without (dashed line) and with (solid line) correction factor

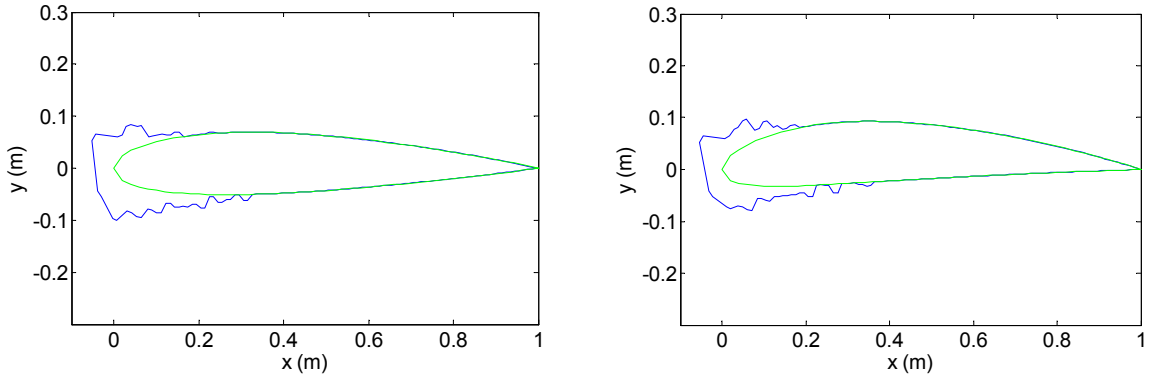

(a) (b)

Fig. 16: Ice on the blade shape obtained (a) without correction factor; (b) with correction factor; under freezing drizzle conditions

The situation under icing conditions could further be improved with a greater value of the correction factor, but it should be kept in mind that the corrected blade shape does not correspond exactly to the performance criteria established for no-icing conditions. The turbine operator may also consider shutting down the wind turbine for the period of icing days or applying a de-icing method when the power output reduces by a great extent due to ice accretion as in the example presented (power 60.3 times smaller than the power produced with the bare blade). In this case, the correction factor would be applied only for the cases when the power output reduces by a lesser extent due to icing so that it is not necessary to shut down the wind turbine. The recommended formula (14) for calculating the correction factor is relatively simple, and it does not consider several factors that influence the icing process or the aerodynamic performance of the wind turbine. Therefore, further study will be beneficial in the future in order to elaborate the method for finding the optimal value of the correction factor.

6. Conclusion

An inverse design process has been developed to obtain a 2D section of wind turbine blades for extreme weather applications. If the prevailing meteorological conditions in the location of the wind turbine justify, then it is recommended modifying the performance criteria defined for no-icing conditions. This means the alteration of the target velocity distribution by the application of a correction factor so that the blade shape obtained by the inverse design process becomes more asymmetric providing greater lift. The application of this blade results in a less severe aerodynamic degradation and power loss by a lesser extent due to ice accretion. The aerodynamic performance of the blades under no-icing and icing conditions have been evaluated by comparing the lift-to-drag ratios of the bare and iced blades, respectively. It was observed that the reduction of lift-to-drag ratio due to ice accretion was most significant for closely symmetric shapes. As the profile becomes more asymmetric, the extent of reduction in this ratio is smaller. According to the results presented, the turbine designer should consider the modification of target velocity distribution and determine its extent (i.e. the value of the correction factor) depending on the prevailing icing conditions in the geographical location of the wind turbine, the frequency of occurrence of the icing event, and the target velocity distribution that was defined for no-icing conditions. Altering the performance criteria to a reasonable extent in the inverse design process modifies the profile of the blade obtained for no-icing conditions so that the wind turbine can operate under some icing conditions as well.

Acknowledgment

This paper was supported by the János Bolyai Research Scholarship of the Hungarian Academy of Sciences. The research was carried out in the frame of the project „EFOP-3.6.1-16-2016-00018 – Improving the role of research + development + innovation in the higher education through institutional developments assisting intelligent specialization in Sopron and Szombathely".

References

[1] O. Parent, A. Ilnica, Anti-icing and de-icing techniques for wind turbines: Critical review, Cold Regions Science and Technology 65 (2011) 88-96.

[2] E. Hau, Wind Turbines: Fundamentals, Technologies, Application, Economics, Springer-Verlag, Berlin, Germany, 2006.

[3] N. Bose, Icing on a small horizontal-axis wind turbine - Part 1: Glaze ice profiles, Journal of Wind Engineering and Industrial Aerodynamics 45 (1992) 75-85.

[4] P. Fu, M. Farzaneh, A CFD approach for modeling the rime-ice accretion process on a horizontal-axis wind turbine, Journal of Wind Engineering and Industrial Aerodynamics 98 (2010) 181-188.

[5] V. Turkia, S. Huttunen, T. Wallenius, Method for estimating wind turbine production losses due to icing, VTT Technology 114 (2013) p. 38.

[6] O. Yirtici, I.H. Tuncer, S. Ozgen, Ice Accretion Prediction on Wind Turbines and Consequent Power Losses, Journal of Physics: Conference Series 753 (2016) p. 10.

[7] A.G. Kraj, E.L. Bibeau, Phases of icing on wind turbine blades characterized by ice accumulation, Renewable Energy 35(5) (2010) 966-972.

[8] H. Seifert, F. Richert, Aerodynamics of Iced airfoils and their Influence on Loads and Power Production, European Wind Energy Conference, Dublin, Ireland, pp. 458-463, 1997.

[9] S. Barber, Y. Wang, N. Chokani, R.S. Abhari, The Effect of Ice Shapes on Wind Turbine Performance, 13th International Workshop on Atmospheric Icing of Structures, Andermatt, Switzerland, 2009.

[10] L. Shu, J. Liang, Q. Hu, X. Jiang, X. Ren, G. Qiu, Study on small wind turbine icing and its performance, Cold Regions Science and Technology 134 (2017) 11-19.

[11] L. Hu, X. Zhu, C. Hu, J. Chen, Z. Du, Wind turbines ice distribution and load response under icing conditions, Renewable Energy 113 (2017) 608-619.

[12] G.M. Ibrahim, K. Pope, Y. S. Muzychka, Effects of blade design on ice accretion for horizontal axis wind turbines, J. Wind Engineering and Industrial Aerodynamics 173 (2018) 39-52.

[13] P. Garabedian, D. McFadden, Design of Supercritical Swept Wings, AIAA Journal 20 (1982) 289-291.

[14] J.B. Malone, J. Vadyak, L.N. Sankar, Inverse Aerodynamic Design Method for Aircraft Components, J. Aircraft 24 (1987) 8-9.

[15] J.B. Malone, R.C. Swanson, Inverse Airfoil Design Procedure Using a Multigrid Navier-Stokes Method, 3rd Int. Conf. on Inverse Design Concepts and Optimization in Engineering Sciences, Washington, DC, USA, pp. 55-66, 1991.

[16] G.S. Dulikravich, D.P. Baker, Fourier Series Solution for Inverse Design of Aerodynamic Shapes, Int. Symp. on Inverse Problems in Engineering Mechanics, Nagano, Japan, pp. 427-436, 1998.

[17] L.E. Kollár, R. Mishra, A. Jain, Inverse Design of Blade Shapes for Vertical Axis Wind Turbines, Proc. 6th Int. and 43rd National Conf. on Fluid Mechanics and Fluid Power, Paper No. 26, Allahabad, India, 2016.

[18] B. Kamoun, D. Afungchui, M. Abid, The inverse design of the wind turbine blade sections by the singularities method, Renewable Energy 31 (2006) 2091-2107.

[19] A. Albanesi, V. Fachinotti, I. Peralta, B. Storti, C. Gebhardt, Application of the inverse finite element method to design wind turbine blades, Composite Structures 161 (2017) 160-172.

[20] S.D. Conte, C. de Boor, Elementary Numerical Analysis, McGraw-Hill, Singapore, 1981.

[21] J.D. Anderson, Fundamentals of Aerodynamics, 3rd Ed., McGraw-Hill, New York, 2001.

[22] L. Makkonen, Models for the growth of rime, glaze, icicles and wet snow on structures, Phil. Trans. R. Soc. Lond. A 358 (2000) 2913-2939.

[23] C.T. Crowe, M.P. Sharma, D.E. Stock, The Particle-Source-In Cell (PSI-CELL) Model for Gas-Droplet Flows, Journal of Fluids Engineering (1977) 325-332.

[24] L.E. Kollár, M. Farzaneh, Modeling the evolution of droplet size distribution in two-phase flows, Int. J. of Multiphase Flow 33 (2007) 1255-1270.

[25] L. Makkonen, T. Laakso, M. Marjaniemi, K.J. Finstad, Modelling and prevention of ice accretion on wind turbines, Wind Engineering 25 (2001) 3-21.

[26] A. Bouhelal, A. Smaili, O. Guerri, C. Masson, Numerical Investigation of Turbulent Flow around a Recent Horizontal Axis Wind Turbine using Low and High Reynolds Models, J. Applied Fluid Mechanics 11(1) (2018) 151-164.

[27] M.O.L. Hansen, Aerodynamics of Wind Turbines, Routledge, Abingdon, UK, 2015.

[28] D.A. Spera, Wind Turbine Technology. Fundamental Concepts of Wind Turbine Engineering, ASME Press, New York, NY, USA, 2009.

[29] E.P. Lozowski, J.R. Stallabras, P.F. Hearty, The Icing of an Unheated, Nonrotating Cylinder. Part I: A Simulation Model, Journal of Climate and Applied Meteorology 22 (1983) 2053-2062.

[30] L.E. Kollár, R. Mishra, Icing of Wind Turbine Blades Obtained by an Inverse Design Process, Digital Proc. 12th Conference on Sustainable Development of Energy, Water and Environment Systems, SDEWES2017.0806, 1-8, Dubrovnik, Croatia, 2017.

Appendix

Flowchart of the computation involving the inverse design process, the air flow field around the bare blade, and the icing of the blade